

High Energy Studies of Pulsar Wind Nebulae

Patrick Slane

Harvard-Smithsonian Center for Astrophysics

Abstract. The extended nebulae formed as pulsar winds expand into their surroundings provide information about the composition of the winds, the injection history from the host pulsar, and the material into which the nebulae are expanding. Observations from across the electromagnetic spectrum provide constraints on the evolution of the nebulae, the density and composition of the surrounding ejecta, the geometry of the systems, the formation of jets, and the maximum energy of the particles in the nebulae. Here I provide a broad overview of the structure of pulsar wind nebulae, with specific examples that demonstrate our ability to constrain the above parameters. The association of pulsar wind nebulae with extended sources of very high energy gamma-ray emission are investigated, along with constraints on the nature of such high energy emission.

Keywords: Pulsar Wind Nebulae; Pulsars; Supernova Remnants

PACS: 01.30.Cc;95.85.Hp;95.85.Bh; 95.85.Nv;95.85.Pw;97.60.Gb;98.38.Mz

It has long been known that the Crab Nebula is produced by the wind from a young, energetic pulsar whose spin-down power manifests itself as a synchrotron-emitting bubble of energetic particles. Optical observations reveal a network of filaments where the nebula has swept up surrounding ejecta from the progenitor star, and an inner shock region where the pulsar wind joins the slower flow in the nebula. Observations from the radio band to the very high energy (VHE) γ -ray band reveal the presence of energetic particles swimming through a bubble of magnetic field and photons, some self-generated, resulting in copious synchrotron and inverse-Compton emission. (For a recent review on the Crab nebula, see Hester 2008.) More recently, it has become clear that this basic structure holds for all pulsar wind nebula (PWNe), and observed variations in their properties provide us with information about differences in their conditions and evolutionary states.

The diagram shown in Figure 1 (inset) illustrates the main points of the most basic picture for a PWN: in an inner zone the wind flows away from the neutron star (NS) with Lorentz factor $\gamma \sim 10^6$; at a distance R_w from the NS the wind passes through a termination shock, decelerating the flow while boosting particle energies by another factor of $\gtrsim 10^3$; and beyond R_w energetic electrons in the wind radiate synchrotron emission in the wound-up toroidal magnetic field to form the PWN which is confined at a radius R_{PWN} by the inertia of the SN ejecta or the pressure of the interior of a surrounding SNR. A detailed theoretical framework, incorporating particle injection and diffusion, magnetic field evolution and radiative and adiabatic losses, has been constructed within this picture, allowing us to successfully predict and explain some basic PWN properties (Reynolds & Chevalier 1984; Kennel & Coroniti 1984). For a more detailed review on the structure and evolution of PWNe,

see Gaensler & Slane (2006).

BROADBAND EMISSION FROM PWNE

The broadband emission from a PWN is determined by the power and spectrum of particles injected by the pulsar, as well as the environment into which the PWN expands. The input luminosity is e.g. Pacini & Salvati (1973)

$$\dot{E} = \dot{E}_0 \left(1 + \frac{t}{\tau_0}\right)^{-\frac{(n+1)}{(n-1)}}, \quad (1)$$

where

$$\tau_0 \equiv \frac{P_0}{(n-1)\dot{P}_0} \quad (2)$$

is the initial spin-down time scale of the pulsar. Here \dot{E}_0 is the initial spin-down power, P_0 and \dot{P}_0 are the initial spin period and its time derivative, and n is the so-called "braking index" of the pulsar ($n = 3$ for magnetic dipole spin-down). The pulsar has roughly constant energy output until a time τ_0 , beyond which the output declines fairly rapidly with time.

Based on studies of the Crab Nebula, there appear to be two electron populations - one corresponding to relic radio-emitting electrons that may have been injected early in the evolution of the supernova, and one associated with electrons injected directly by the pulsar wind (Atoyan & Aharonian 1996). These are often parameterized as a broken power law:

$$Q(E_e, t) = Q_0(t)(E_e/E_b)^{-\alpha} \quad (3)$$

with $\alpha = \alpha_1$ for $E_e < E_b$ and $\alpha = \alpha_2$ for $E_e \geq E_b$. Here E_b represents the energy of a spectral break due to the

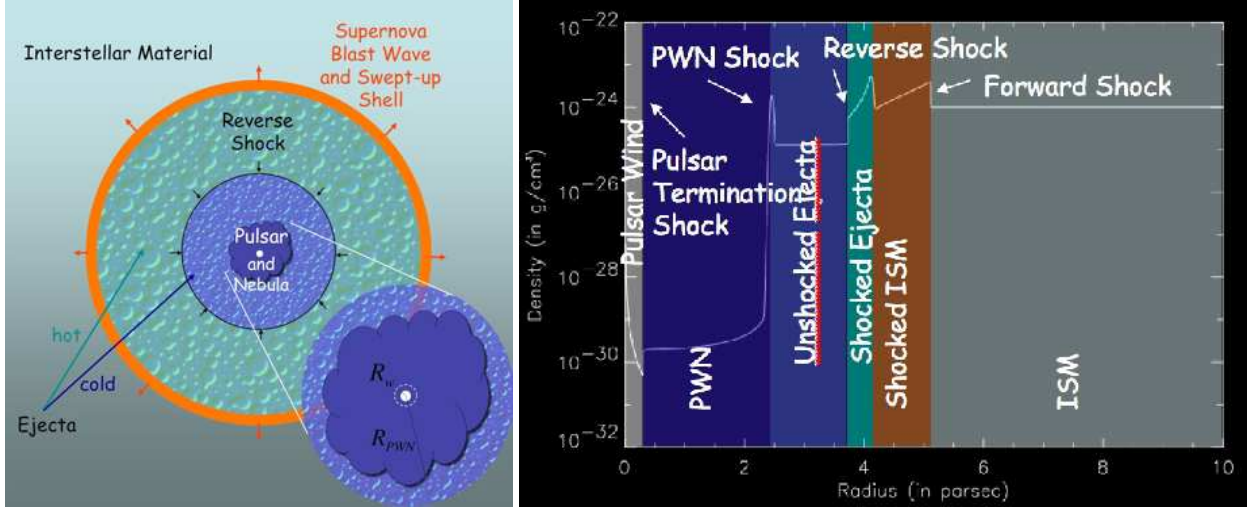


FIGURE 1. Left: Conceptual diagram of a PWN within an SNR, illustrating the central pulsar and nebula, surrounding cold ejecta, shock-heated ejecta, and surrounding medium. Right: Density structure within a composite SNR, identifying the discrete zones illustrated in the schematic diagram. The position of the forward and reverse shocks that heat the CSM/ISM and ejecta are shown, along with that of the PWN shock that expands into cold ejecta, and that of the pulsar wind termination shock. See text for a detailed description.

two distinct populations. The integrated energy in the electron spectrum is then

$$\int Q(E, t) E dE = (1 + \sigma) \dot{E}(t) \quad (4)$$

where σ is the ratio of the spin-down power injected in the form of Poynting flux to that in the form of particles.

The electrons injected into the PWN produce synchrotron radiation in the nebular magnetic field, as well as inverse-Compton (IC) emission by upscattering photons from the cosmic microwave background (CMB), ambient starlight, and emission from nearby dust. The resulting emission spectrum is found by integrating the electron spectrum over the emissivity function for synchrotron and inverse-Compton radiation (e.g. Lazendic et al. 2004) using, respectively, the nebular magnetic field and spectral density of the ambient photon field. For electrons of energy E_{TeV} (in units of TeV), the mean energy for synchrotron-emitted photons is

$$\epsilon_s \approx 2 \times 10^{-4} E_{TeV}^2 B_{-5} \text{ keV}, \quad (5)$$

where B_{-5} is the magnetic field strength in units of 10^{-5} G, while the average IC-scattered photon from the CMB has energy

$$\epsilon_{ic} \approx 3 \times 10^{-3} E_{TeV}^2 \text{ TeV}. \quad (6)$$

For a typical PWN power law particle spectrum, the ratio of the synchrotron and IC fluxes at these energies depends primarily on the magnetic field strength (Aharonian & Atoyan 1999):

$$\frac{f_{ic}(\epsilon_{ic})}{f_s(\epsilon_s)} \approx 0.1 B_{-5}^{-2} \quad (7)$$

where $f(E) = E^2 dF/dE$. The ratio of the peak $f(E)$ values for the spectra, shown schematically in Figure 2, is thus an indicator of the magnetic field strength.

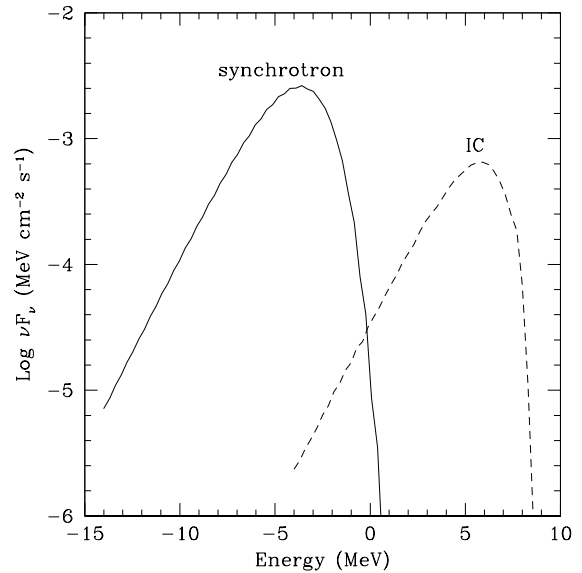


FIGURE 2. Illustration of the synchrotron and inverse-Compton emission from a power law distribution of particles. Here we have used an exponential cutoff at the high energy end of the particle distribution, a power law index of 2.4, and magnetic field of $5\mu\text{G}$. IC scattering is from the CMB, and the particle spectrum normalization is arbitrary.

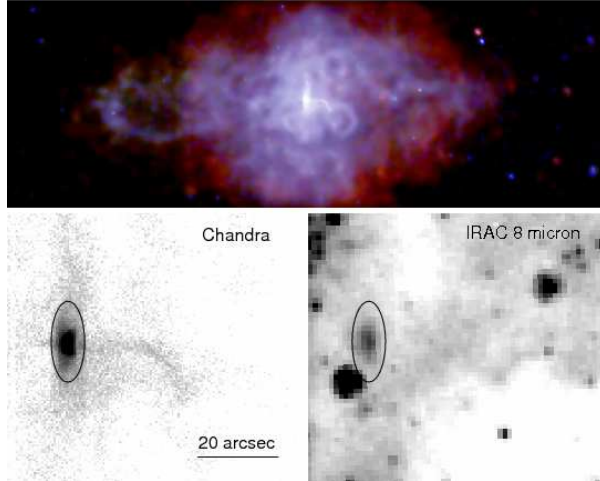


FIGURE 3. Upper: *Chandra* image of 3C 58 showing a complex of filamentary structures embedded in a large-scale nebula. The pulsar is at the center, accompanied by torus and jet-like structures. Lower: *Chandra* image of the pulsar, torus, and jet (left), along with *Spitzer* image revealing emission from the torus at $8\mu\text{m}$.

From the above, we see that for $B \sim 150\mu\text{G}$, electrons that produce 1 TeV photons from IC scattering of the CMB will produce 1 keV synchrotron photons. For lower magnetic fields, the X-ray-emitting electrons are more energetic than the γ -ray-emitting electrons. An important result is that for low magnetic fields and large ages, synchrotron losses can result in a cooling break in the electron spectrum that falls below the X-ray-emitting regime. The result is a PWN that has very little X-ray emission, but is bright in the VHE γ -ray band. This is discussed further below.

The evolution of the PWN spectrum is determined by balance of injection and losses,

$$\frac{dn_e(E_e, t)}{dt} = Q(E_e) - \frac{n_e(E_e, t)}{\tau_{rad}} - \frac{n_e(E_e, t)}{\tau_{esc}} \quad (8)$$

where τ_{rad} and τ_{esc} are timescales for radiative and escape losses, as well as the evolution of the magnetic field. Venter & de Jager (2006) parameterize the latter as

$$B(t) = \frac{B_0}{1 + (t/\tau_B)^\xi} \quad (9)$$

where τ_B is a characteristic timescale connected to the input history of the pulsar, and ξ is a free parameter.

Applying the above to the emission from a nebula of known age and spin-down power provides constraints on the initial pulsar spin period and magnetic field strength in the nebula, and has been used successfully in modeling emission from a number of systems including the Crab Nebula, the PWN associated with PSR B1509–58, and

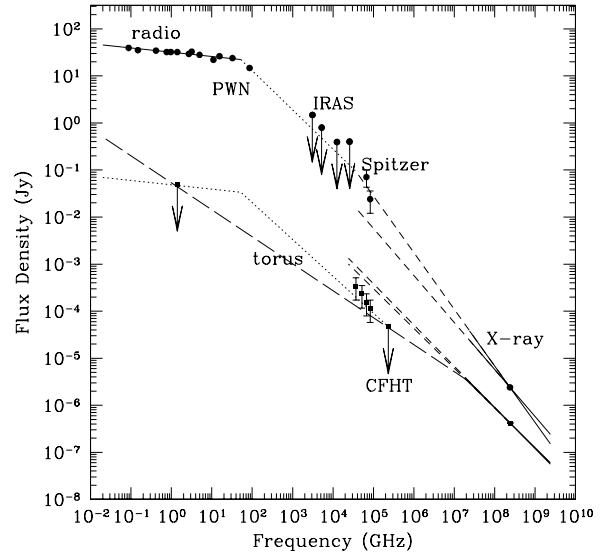


FIGURE 4. The flux of all of 3C 58 (upper) and its torus (lower), plotted from the radio to the X-ray band. While the torus is not detected in the radio band, the IR data require a flattening of the X-ray spectrum when extrapolated back to the longer wavelength band.

G0.9+0.1 (Venter & de Jager 2006; Zhang et al. 2008). It is important to note that this describes a spatially-averaged spectrum for the nebula, with no consideration given to variations of the magnetic field, for example. A more complete treatment of the nebula structure, in which the particles emerge from a termination shock in the form of an axisymmetric particle and magnetic wind, which is allowed to evolve through radiative and adiabatic losses in order to determine the magnetic field distribution and electron spectrum, is required to address spatial and spectral variations observed in high resolution observations of PWNe. Recent work in this area has revolutionized our understanding of the inner structure of PWNe (e.g. Lyubarsky 2002, Komissarov & Lyubarsky 2004), and extensions to include the associated emissivity have now produced both detailed emission maps and broadband spectral energy distributions based on these more encompassing models (e.g. del Zanna et al., Volpi et al).

A Point About Injection: 3C 58

While most attempts to model the emission and evolution of PWNe start with the assumption that a power law particle spectrum is injected into the nebula at the wind termination shock, there is evidence that the spectrum may be more complicated. Low-frequency spec-

tral breaks are observed in a number of PWNe, including 3C 58 and G21.5-0.9, for example. If interpreted as cooling breaks, these would require uncomfortably large magnetic fields (Green & Scheuer 1992). Instead, it has been suggested that these are the result of either an episodic change in the pulsar input at an earlier epoch (e.g. Woljter et al. 199x) or an intrinsic feature in the injection spectrum (Frail 1998).

Chandra Observations of 3C 58 (Slane et al. 2004) reveal an extended nebula filled with a complex of loop-like structures and surrounded by a shell of swept-up ejecta (Figure 3). At the center is an energetic young pulsar accompanied by a jet and surrounded by a toroid that is also observed with *Spitzer* observations (Slane et al. 2008). These observations, combined with data from other wavebands, show that the spectrum emerging from the wind termination shock in this system requires one or more spectral breaks (Figure 3). Such breaks will imprint themselves on the broadband spectra of PWNe, causing the emission to deviate from that expected from a pure power law input, and potentially producing the low energy breaks observed for the large scale nebula, such as that seen in 3C 58 (Figure 3). Consideration must be given to such complexities in the injection spectrum to properly understand the evolution of the broadband spectrum.

EVOLUTION OF PWNE WITHIN SNRS

Since a pulsar is formed in a supernova explosion, the star and its PWN are initially surrounded by the expanding ejecta and swept-up circumstellar material that comprise the associated SNR. At early times the SNR blast wave expands rapidly ($v_s > (5 - 10) \times 10^3 \text{ km s}^{-1}$), while the pulsar itself moves at a slower (but often significant) speed (with typical magnitude $\sim 400 \text{ km s}^{-1}$) as the result of a “kick” due to asymmetries in the explosion. In the early phases of evolution, the pulsar is thus located very near the center of the SNR.

The energetic wind is injected into the SNR interior, forming a high-pressure bubble that expands supersonically into the surrounding ejecta, forming a shock. The radius of the PWN evolves as

$$R_{PWN} \approx 1.5 \dot{E}_0^{1/5} E_{SN}^{3/10} M_{ej}^{-1/2} t^{6/5} \quad (10)$$

where E_{SN} is the energy released in the explosion and M_{ej} is the mass of the ejecta (Chevalier 1977). Thus, at least at early times when the pulsar input is high, the PWN expansion velocity increases with time. The sound speed in the relativistic fluid within the PWN is sufficiently high ($c_s = c/\sqrt{3}$) that any pressure variations experienced during the expansion are quickly balanced within the bubble; at early stages, we thus expect the

pulsar to be located at the center of the PWN. The pressure balance within the PWN results in a termination shock where the energetic pulsar wind meets the more slowly-expanding PWN.

The outer blast wave of the SNR, meanwhile, drives a shock into the surrounding interstellar/circumstellar medium (ISM/CSM), forming a shell of hot gas and compressed magnetic field. As the shell sweeps up additional mass, and decelerates, a reverse shock (RS) propagates back into the expanding ejecta. As illustrated in Figure 1, the entire system is thus described by four shocks: a forward shock that sweeps up the CSM/ISM; a reverse that heats the supernova ejecta (which is initially cold due to severe adiabatic losses from the rapid expansion); a shock at the PWN/ejecta boundary, where the expanding nebula compresses and heats surrounding ejecta; and the pulsar wind termination shock. At early times, the SNR reverse shock expands outward, but more slowly than the forward shock, but eventually it moves inward. In the absence of a central pulsar or PWN, the reverse shock reaches the center of the SNR in a time

$$t_c \approx 7 \left(\frac{M_{ej}}{10 M_\odot} \right)^{5/6} \left(\frac{E_{SN}}{10^{51} \text{ ergs}} \right)^{-1/2} \left(\frac{n_0}{\text{cm}^{-3}} \right)^{-1/3} \text{ kyr}, \quad (11)$$

where n_0 is the number density of ambient gas (Reynolds & Chevalier 1984).

RS/PWN INTERACTIONS

In the presence of a young pulsar, the reverse shock collides with the expanding PWN at a time

$$t_{col} \approx 1045 E_{51}^{-1/2} \left(\frac{M_{ej}}{M_\odot} \right)^{5/6} n_0^{-1/3} \text{ yr} \quad (12)$$

where E_{51} is the explosion energy in units of 10^{51} erg (van der Swaluw et al. 2004). This compresses the PWN until the pressure in the nebula is sufficiently high to rebound, and again expand into the ejecta. The system goes through several reverberations over the course of several tens of thousands of years.

The crushing of the PWN results in an increase in the magnetic field. This causes a rapid burn-off of the most energetic particles in the nebula. The PWN/RS interface is Rayleigh-Taylor unstable, and is subject to the formation of filamentary structure where the dense ejecta material is mixed into the relativistic fluid (Blondin et al. 2001). The nebula subsequently re-forms as the pulsar injects fresh particles into its surroundings, but a significant relic nebula of mixed ejecta and relativistic gas will persist.

In cases where the pulsar and its PWN have moved considerably from the center of the PWN, or in which

the SNR has evolved in a medium of nonuniform density, the reverse shock will interact with the PWN asymmetrically, encountering one portion of the nebula well before another. This results in a complex interaction that leaves a highly distorted relic nebula that may be highly displaced from the pulsar position (Blondin et al. 2001).

PWNE AS EXTENDED VHE γ -RAY SOURCES

Recent observations with the latest generation of VHE γ -ray telescopes have uncovered a large number of sources that are, or appear to be, associated with PWNe. As described above, the broadband spectra provide strong constraints on the structure and magnetic fields in these systems. Coupled with information about their angular sizes, distances, and associations with any identified compact objects or supernova remnants, these observations are providing new insights into PWN evolution. Here I summarize results from three such studies that illustrate some of the key results that have been obtained.

HESS J1640–465

HESS J1640-465 (Aharonian et al. 2006a) was identified as an extended source of VHE γ -ray emission in a survey of the inner Galaxy carried out by *H.E.S.S.* in 2004-2006. The source has a radius of ~ 3 arcmin, and the spectrum is well-described by a power law with an index of ~ 2.4 . The source is spatially coincident with G338.3–0.0, a shell-type SNR with a diameter of ~ 8 arcmin (Figure 5, top). The peak of the γ -ray emission falls interior to the radio shell, suggesting that the emission may be from a pulsar-powered nebula associated with the SNR, although no known pulsar resides in this vicinity.

X-ray observations with *XMM-Newton* (Funk et al. 2007) reveal extended X-ray emission in the central regions of HESS J1640-465, suggestive of a PWN core. Subsequent *Chandra* observations (Lemiere et al. 2008) reveal a compact object surrounded by a faint diffuse nebula (Figure 5, top inset) whose nonthermal X-ray spectrum shows clear evidence for steepening with radius, as expected if strong synchrotron losses have prevented energetic electrons from diffusing to large distances from the putative pulsar.

HI absorption measurements (Lemiere et al. 2008) establish a distance of 8 - 13 kpc for G338.3–0.0, suggesting an age for the system of 10 - 30 kyr. Based on the X-ray luminosity of $\sim 4 \times 10^{33} d_{10}^2$ erg s $^{-1}$ for the X-ray nebula (where d_{10} is the distance in units of 10 kpc), a typical efficiency of $\sim 0.1\%$ for conversion of spin-down power to X-ray emission suggests $\dot{E} \sim 4 \times 10^{33}$ erg s $^{-1}$

for the putative pulsar. Using the approach described in Section 2, a leptonic model can adequately describe the X-ray and γ -ray spectra, and predicts a system age of ~ 15 kyr with a mean magnetic field strength of $\sim 6\mu\text{G}$.

The observed position and morphology of the X-ray nebula associated with HESS J1640–465 is somewhat perplexing. It is not at the center of the SNR shell, and the extended emission is not symmetric about the position of the putative pulsar. If born at the geometric center of G338.3–0.0, its current position indicates a projected space velocity of ~ 500 km s $^{-1}$, which is not unreasonable for a pulsar. However, the asymmetric shape of the diffuse nebula makes such an explanation problematic. A more likely scenario may be that the PWN has already undergone disruption from the RS interaction. Based on the distribution and kinematics of the molecular and neutral gas in this vicinity, it appears likely that the SNR has evolved in a sufficiently complex environment to expect an asymmetric RS/PWN interaction (Lemiere et al. 2008).

HESS J1825–137

Also discovered as part of the *H.E.S.S.* Galactic plane survey, HESS J1825–137 is a large-diameter ($\sim 1^\circ$) γ -ray source with a highly asymmetric morphology (Figure 5, bottom). It is apparently associated with the PSR B1823–13, located at a distance of ~ 4 kpc. The pulsar has a spin-down power $\dot{E} = 2.8 \times 10^{36}$ erg s $^{-1}$ and is surrounded by a faint X-ray nebula (see Figure 5, bottom inset) whose extended morphology, similar in orientation to that of HESS J1825–137 but on a much smaller scale, suggests that the PWN has been disrupted by the SNR reverse shock (Gaensler et al. 2003). This is consistent with the significant offset between the pulsar and the geometric center of HESS J1825–137.

Remarkably, the radius of HESS J1825–137 is observed to decrease with increasing energy in the γ -ray band, providing the first evidence in this band for the effects of synchrotron burn-off on the underlying electron spectrum. Variations in the emission spectrum confirm a spectral steepening with radius, as expected from such losses. These observations imply a magnetic field strength of only $\sim 2 - 4\mu\text{G}$, and an age of $\sim 20 - 40$ kyr (de Jager & Djannati-Ataï).

The extremely large size of HESS J1825–137 makes this the largest PWN known. With a radius of nearly 35 pc, it appears clear that the system has evolved well past the reverse-shock crossing phase, and that the PWN has rebounded and continued to expand within its unseen host SNR. The spectral steepening seen in the *H.E.S.S.* data suggest that the radiative loss break has progressed to energies well below X-ray-emitting values, thus ex-

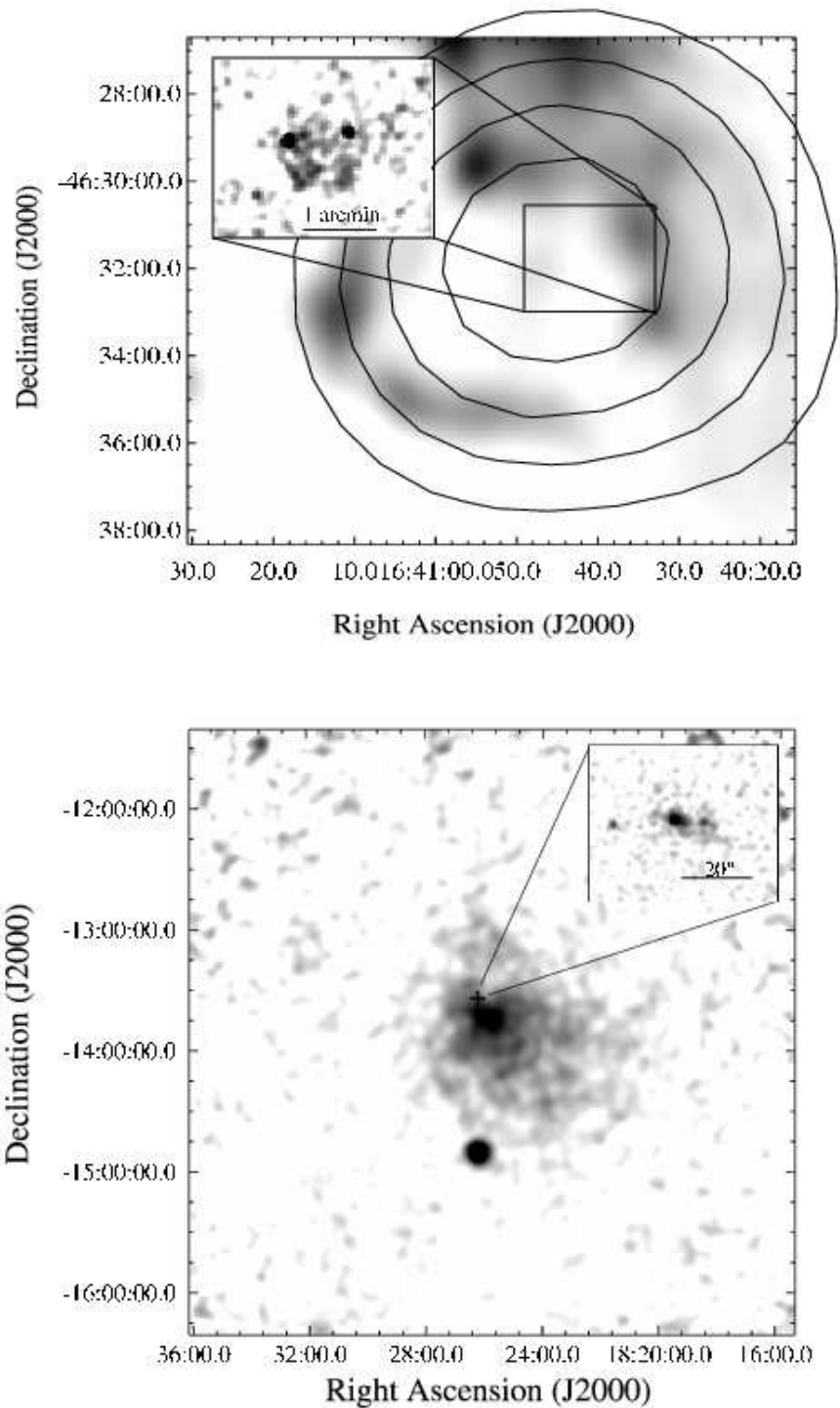


FIGURE 5. Upper: Radio image of G338.3-0.0 with contours from HESS J1640-465. The inset shows the *Chandra* image of the central regions, revealing the putative pulsar (the brightest source in the field) surrounded by a faint extended X-ray nebula. Lower: H.E.S.S. image of J1825-137. The cross marks the position of PSR B1823-13 and the inset shows the *Chandra* image of the pulsar, revealing a faint extended nebula.

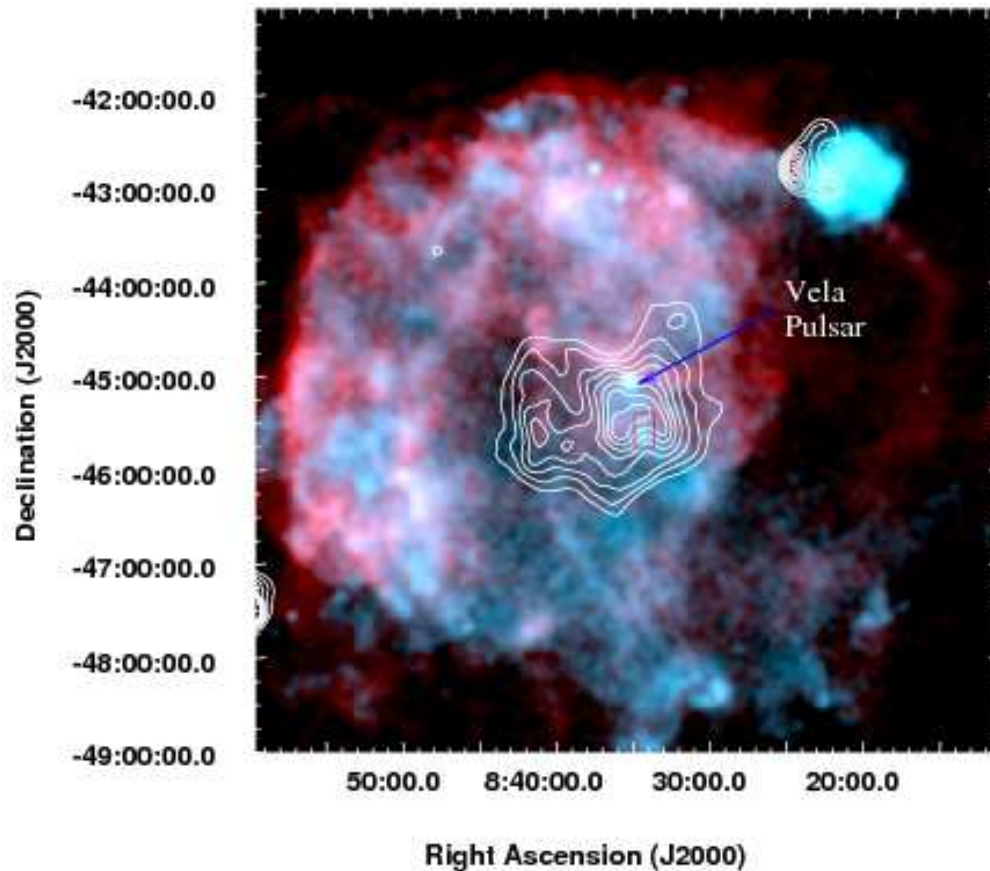


FIGURE 6. *ROSAT* image of the Vela SNR. Radio emission from the associated PWN Vela X is shown with contours. The pulsar is indicated with an arrow, and is offset from the center of Vela X, presumably due to the reverse shock interaction. Hard X-ray emission, shown in blue, extends southward from the pulsar, into Vela X, and this structure is accompanied by VHE γ -ray emission. The red box indicates the region from which *XMM-Newton* spectra were extracted (see text and Figure 7).

plaining the lack of X-ray emission from sites other than very near the pulsar, where fresh particle injection is taking place. The properties of HESS J1825–137 suggest that there may be a significant population of γ -ray-bright sources with very faint or undetectable counterparts – perhaps providing an explanation for the emerging number of “dark” TeV sources (de Jager & Djannati-Ataï 2008).

Vela X

The Vela supernova remnant (Figure 6) is a prototype of the composite class in which the shell of hot gas swept up by the forward shock of the explosion is accompanied

by a nonthermal nebula driven by the pulsar formed in the collapse of the progenitor star. The SNR shell is quite cool, indicating an object of moderate age, and fragments of metal-rich ejecta that have overtaken the decelerated blast wave are observed well outside the shell. The pulsar itself is accompanied by a compact jet-torus structure that provides the direction of the pulsar spin axis, and the extended wind nebula – identified with the large radio region known as Vela X – is located predominantly to the south of the pulsar, apparently having been disrupted by the reverse shock in the remnant.

ROSAT observations of the Vela X region (Markwardt & Ögelman 1995) reveal a large emission structure extending to the south of the pulsar (Figure 8). The region is characterized by a hard spectrum and appears to lie along a bright elongated radio structure (Frail et al. 1997). Ob-

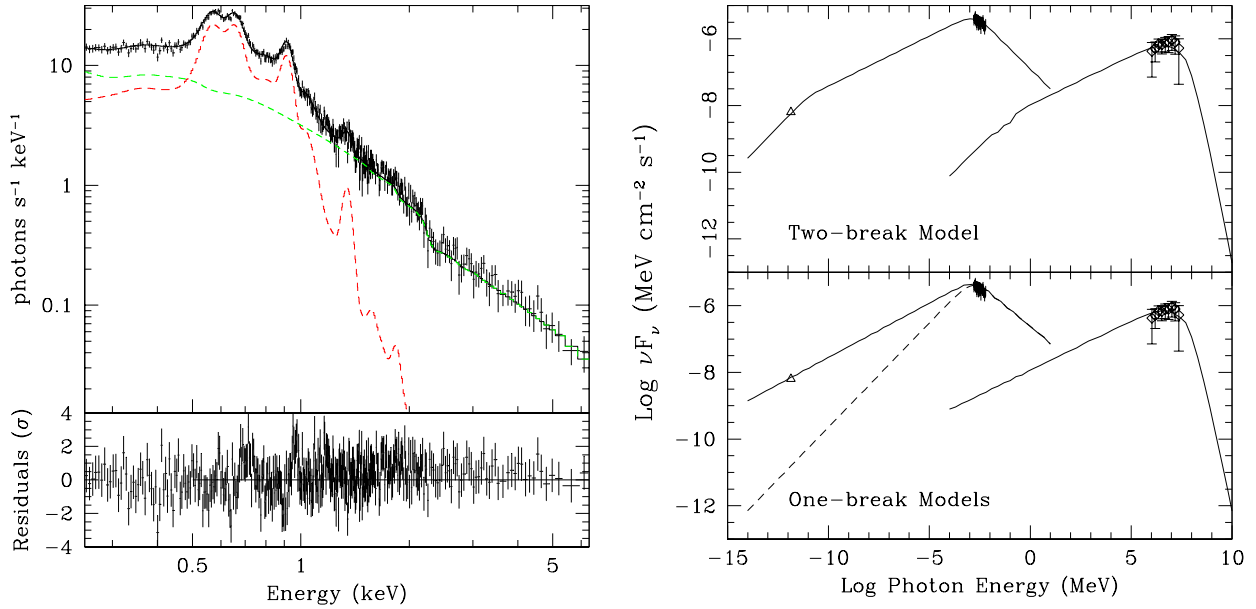


FIGURE 7. Left: *XMM-Newton* spectrum from the “cocoon” region in Vela X. The best-fit model, shown in black, is composed of two components – a thermal plasma with enhanced, ejecta-like abundances (shown in red) and a power law (shown in green). Right: Broadband spectral model consisting of synchrotron emission in the radio and X-ray bands accompanied by inverse-Compton emission in the VHE γ -ray band. The upper panel shows a model with two spectral breaks in the electron spectrum. Models with a single break (lower panel) either underpredict the radio emission, or produce a radio flux whose spectral index does not agree with observations. (From LaMassa et al. 2008.)

servations with *H.E.S.S.* reveal bright VHE γ -ray emission from a region extending directly along this feature (Aharonian et al. 2006b).

Spectral studies carried out with *XMM-Newton* (LaMassa et al. 2008) reveal two distinct emission components in the X-ray band – a power law with a spectral index of ~ 2.2 and a thermal plasma with enhanced abundances of O, Ne, and Mg, presumably associated with ejecta that has been mixed into the PWN upon its interaction with the reverse shock. The derived density of the thermal-emitting, ejecta-rich gas is $n \sim 0.06 \text{ cm}^{-3}$, too low to accommodate hadronic scenarios for the γ -ray emission.

A leptonic model consisting of a broken power law for the electrons in this region of the nebula is able to successfully reproduce the broadband emission as a combination of synchrotron radiation in the radio and X-ray bands, and inverse-Compton scattering of the cosmic microwave background from the same electron population to produce the γ -ray emission (Figure 8). The best-fit model requires a magnetic field strength of $\sim 5 \mu\text{G}$ and an electron spectrum with two spectral breaks. The lower break is presumably intrinsic to the injected electron spectrum, or corresponds to a distinct population of radio-emitting particles injected early in the formation of the PWN, while the upper break is presumably asso-

ciated with synchrotron cooling of the electrons. Models with a single break are also possible, but violate either the observed radio flux or its spectral index (LaMassa et al. 2008)

Our understanding of the low-energy electron spectrum in Vela X is severely limited by the lack of observations at frequencies beyond about 30 GHz. It is unclear whether the spectrum has a break in this region, as suggested above, or continues to higher energies as a distinct population. However, electrons that would produce emission beyond the current radio frequency limits will also upscatter ambient photons into the energy sensitivity range of the *Fermi* LAT (de Jager et al. 2008). Indeed, modeling shows that the three distinct photon populations (the CMB, ambient starlight, and IR emission from ambient dust) will produce discrete and resolvable features in the LAT. Future results from the ongoing LAT sky survey thus promise to address key questions about the particle distribution in Vela X. This, combined with more extensive studies of the thermal and nonthermal X-ray emission will place strong constraints on the full evolution of Vela X, from the formation stage through the process of reverse-shock crushing of the PWN.

SUMMARY

The broadband spectra of PWNe provide information about both the structure and evolution of these objects. New measurements in the VHE γ -ray band, combined with detailed measurements provided by radio and X-ray studies, have begun to reveal information about the earliest stages of particle injection in PWNe as well as a view to the late-phase evolution characteristics. These sources currently represent a significant fraction of the known VHE γ -ray sources, and future observations, combined with those from *Fermi* are sure to extend this new frontier. Complemented by multiwavelength observations, these results promise to extend the current flourish of activity in observational and theoretical work on pulsar winds.

ACKNOWLEDGMENTS

The author acknowledges significant contributions to this work by B. Gaensler, S. Reynolds, D. Helfand, J. Gelfand, O. C. de Jager, S. LaMassa, and A. Lemièrè. Partial support was provided by NASA Contract NAS8-03060.

REFERENCES

1. F. Aharonian and A. M. Atoyan *A&A* **351**, 330 (1999).
2. F. Aharonian, et al., *A&A* **460**, 489 (2006a).
3. F. Aharonian, et al., *A&A* **448**, L43 (2006b).
4. J. M. Blondin, R. A. Chevalier, and D. M. Frierson, *ApJ* **563**, 806 (2001).
5. R. A. Chevalier, *In Supernovae, ed. DN Schramm, pp. 53-61. Dordrecht:Reidel* (1977).
6. O. C. de Jager and A. Djannati-Ataï, *arXiv:0803.0116v1* (2008).
7. O. C. de Jager, P. Slane, and S. M. LaMassa, *ApJ* in press (2008).
8. L. Del Zanna, D. Volpi, E. Amato, and N. Bucciantini, *A&A* **453**, 621 (2006).
9. D. A. Frail, *In "The Many Faces of Neutron Stars." Edited by R. Bucccheri, J. van Paradijs, and M. A. Alpar. Dordrecht ; Boston : Kluwer Academic Publishers, 1998., p.179* (1998).
10. D. A. Frail et al., *ApJ* **475**, 224 (1997).
11. S. Funk et al., *ApJ* **267**, 517 (2007).
12. B. M. Gaensler et al., *ApJ* **588**, 441 (2003).
13. B. M. Gaensler and P. O. Slane, *ARA&A* **44**, 17 (2006).
14. D. A. Green and P. A. G. Scheuer, *MNRAS* **258**, 833 (1992).
15. J. J. Hester, *ARA&A* **46**, 127 (2008).
16. C. F. Kennel and F. V. Coroniti, *ApJ* **283**, 694 (1984).
17. S. Komissarov and Y. E. Lyubarsky, *Ap&SS* **293**, 107 (2004).
18. S. M. LaMassa, P. O. Slane, and O. C. de Jager, *ApJ* in press (2008).
19. J. S. Lazendic et al., *ApJ* **602**, 271 (2004).
20. A. Lemièrè et al., *ApJ* submitted (2004).
21. Y. E. Lyubarsky, *MNRAS* **329**, L34 (2002).
22. C. Markwardt and H. Ögelman, *Nature* **375**, 40 (1995).
23. F. Pacini and M. Salvati, *ApJ* **186**, 249 (1973).
24. S. P. Reynolds, and R. A. Chevalier, *ApJ* **278**, 630 (1984).
25. P. Slane et al., *ApJ* **616**, 403 (2004).
26. P. Slane et al., *ApJ* **676**, L33 (2008).
27. C. Venter and O. C. de Jager, *astro.ph.12652* (2006).
28. E. van der Swalum, T. P. Downes, and R. Keegan, *A&A* **420**, 937 (2004).
29. D. Volpi, L. Del Zanna, E. Amato, and N. Bucciantini, *A&A* **485**, 337(2008).
30. L. Woltjer, M. Salvati, F. Pacini, and R. Bandiera, *A&A* **325**, 295 (1997).
31. L. Zhang, S. B. Chen, and J. Fang, *ApJ* **676**, 1210 (2008).